# Trends in Stratospheric Ozone: Lessons Learned from a 3D Chemical Transport Model

RICHARD S. STOLARSKI AND ANNE R. DOUGLASS

*Atmospheric Chemistry and Dynamics Branch, NASA Goddard Space Flight Center, Greenbelt, Maryland*

STEPHEN STEENROD

*Science Systems Applications, Inc., Lanham, Maryland*

STEVEN PAWSON

*Global Modeling and Assimilation Office, NASA Goddard Space Flight Center, Greenbelt, Maryland*

(Manuscript received 22 March 2005, in final form 7 July 2005)

ABSTRACT

Stratospheric ozone is affected by external factors such as chlorofluorcarbons (CFCs), volcanoes, and the 11-yr solar cycle variation of ultraviolet radiation. Dynamical variability due to the quasi-biennial oscillation and other factors also contribute to stratospheric ozone variability. A research focus during the past two decades has been to quantify the downward trend in ozone due to the increase in industrially produced CFCs. During the coming decades research will focus on detection and attribution of the expected recovery of ozone as the CFCs are slowly removed from the atmosphere. A chemical transport model (CTM) has been used to simulate stratospheric composition for the past 30 yr and the next 20 yr using 50 yr of winds and temperatures from a general circulation model (GCM). The simulation includes the solar cycle in ultraviolet radiation, a representation of aerosol surface areas based on observations including volcanic perturbations from El Chichon in 1982 and Pinatubo in 1991, and time-dependent mixing ratio boundary conditions for CFCs, halons, and other source gases such as $N_2O$ and $CH_4$. A second CTM simulation was carried out for identical solar flux and boundary conditions but with constant "background" aerosol conditions. The GCM integration included an online ozonelike tracer with specified production and loss that was used to evaluate the effects of interannual variability in dynamics. Statistical time series analysis was applied to both observed and simulated ozone to examine the capability of the analyses for the determination of trends in ozone due to CFCs and to separate these trends from the solar cycle and volcanic effects in the atmosphere. The results point out several difficulties associated with the interpretation of time series analyses of atmospheric ozone data. In particular, it is shown that lengthening the dataset reduces the uncertainty in derived trend due to interannual dynamic variability. It is further shown that interannual variability can make it difficult to accurately assess the impact of a volcanic eruption, such as Pinatubo, on ozone. Such uncertainties make it difficult to obtain an early proof of ozone recovery in response to decreasing chlorine.

## 1. Introduction

Stratospheric ozone is produced by ultraviolet photodissociation of molecular oxygen and destroyed by catalytic reactions of the oxides of hydrogen, nitrogen, chlorine, and bromine. The distribution of ozone with latitude, longitude, and altitude is determined by large- and small-scale transport between regions of net production and regions of net loss. Stratospheric ozone is sensitive to variability in both photochemical and dynamical processes and thus varies on seasonal and longer time scales. After accounting for variability due to the seasonal and solar cycle in ultraviolet flux, variability due to volcanic aerosols, and variability due to dynamic influence such as the quasi-biennial oscillation (QBO), analysis of observations indicate a downward trend in stratospheric ozone over the time period from 1979 to the late 1990s (Stolarski et al. 1991; Harris et al. 1998; Ajavon et al. 2003). The growth of reactive chlorine and bromine in the stratosphere due to decompo-

*Corresponding author address:* Dr. Richard Stolarski, NASA GSFC, Code 613.3, Greenbelt, MD 20771.
E-mail: stolar@polska.gsfc.nasa.gov

© 2006 American Meteorological Society

sition of industrially produced chlorofluorcarbons (CFCs), halons, and methyl bromide has, over the last two decades, led to a decrease in the amount of ozone overhead. The statistical analysis accounts for random and coherent dynamical variability other than the QBO only in the noise term that helps to evaluate uncertainties. Disagreement persists on the quantification of the chemical and dynamical contributions to the trend derived from observations. Several investigators estimate a significant contribution of variations in the dynamics of the stratosphere to the observed trend (Hood et al. 1997; Ziemke et al. 1997; Fusco and Salby 1999; Petzoldt 1999; Weiss et al. 2001; Hadjinicolaou et al. 2002; Randel et al. 2002; Salby and Callaghan 2002).

We seek to accurately predict the course of future ozone recovery as the provisions of the Montreal Protocol and its amendments lead to the slow removal of chlorine from the stratosphere. Our best method to evaluate such predictions is to simulate the past evolution of ozone under the varying natural and anthropogenic influences, and compare such simulations with observations of ozone and other gases. We have completed a three-dimensional simulation using our chemical transport model (CTM) for the years 1973–2022. The simulation includes time-dependent mixing ratios for industrially and naturally produced compounds (e.g., CFCs, halons, methyl bromide, nitrous oxide, methane), and the 11-yr cycle in solar ultraviolet radiation. Volcanic aerosols specified for the time period are based on observations; thus, the abrupt increase and decay of aerosols following eruption of El Chichon and Mt. Pinatubo are appropriately represented. The future projections assume a background level of aerosols. This paper focuses on the years from 1975 to 2003 and the comparison of simulated ozone profiles and total ozone column content with observations. We focus on the comparison of the deduced trends, solar cycle, and volcanic aerosol impacts in the simulation to those deduced from data. In the following sections, we describe the Goddard Space Flight Center Chemistry and Transport Model (GSFC CTM), the observations that are included in this study, and the statistical model used in the analysis. We apply the same time series analysis to the model output and to the data as done earlier by Hadjinicolaou et al. (2002). This is followed by a presentation of the results of application of the statistical time series analysis to the simulated and observed total column ozone, and then the results of application of the same statistical model to simulated and observed ozone profiles. The final section includes discussion of the results and conclusions.

## 2. The GSFC CTM model

The GSFC CTM used here is an updated version of that used by Douglass et al. (2003). The CTM solves a coupled set of constituent continuity equations. Winds and temperatures needed for transport and photochemical reaction rates and photolysis cross sections are input to the CTM; thus, there are no feedbacks between constituents such as ozone and the meteorological fields. Photochemical production and loss are calculated using the stratospheric photochemical scheme described by Douglass and Kawa (1999) and updated by Douglass et al. (2001), using rate constant data from Jet Propulsion Laboratory (JPL) Evaluation 14 (Sander et al. 2003). Numerical transport is calculated using the scheme described by Lin and Rood (1996). A 15-min time step is used for transport and photochemistry. The photolysis rates are calculated using temperature-dependent cross sections (Sander et al. 2003) and reduced fluxes that are interpolated using a lookup table based on detailed radiative transfer calculations (Anderson and Lloyd 1990). The photolysis rates calculated in this way agree with the photolysis benchmark that was developed as part of the Atmospheric Effects of Aviation Project (Stolarski et al. 1995). The CTM accounts for processes involving polar stratospheric clouds using the parameterization described by Considine et al. (2000). The parameterization accounts for denitrification through polar stratospheric cloud (PSC) sedimentation, and accounts for different types of PSCs.

Ozone that is produced in the troposphere is calculated as a separate constituent from ozone that is produced in the stratosphere. We obtain an estimate of tropospheric ozone from the monthly production and loss frequency saved from a simulation for 2001 using the Harvard Goddard Earth Observing System (GEOS) CHEM-tropospheric CTM with meteorological input from the GEOS-3, a version of the GEOS data assimilation system (Fiore et al. 2003). These production and loss terms are repeated each year. Ozone of stratospheric origin that is transported to the troposphere is subject to this tropospheric loss; tropospheric ozone that is transported to the stratosphere is subject to stratospheric loss. The ozone calculated in this way exhibits the main features of the tropospheric climatology developed by Logan (1999).

Surface boundary conditions for source gases including CFCs, halons, methane, and nitrous oxide were specified following scenario A2 of the *Scientific Assessment of Ozone Depletion: 2002* (Ajavon et al. 2003). The solar radiation for 1973–2003 was specified following the procedure described by Chandra et al. (1995).

Empirical relationships, in one nanometer spectral intervals, were derived using ultraviolet solar flux measured by the Solar Ultraviolet Spectral Irradiance Monitor (SUSIM; Brueckner et al. 1993) for 1992–2003 and ground-based measurements of the 10.7-cm radio flux at Ottawa (F10.7). The solar radiation for 1973–2003 was computed using these relationships and the observed F10.7 solar flux. The solar radiation for 2004–23 repeats the 11-yr solar cycle for 1992–2003. The aerosol distribution was specified from a monthly mean climatology based on satellite data, similar to that used by Jackman et al. (1996) and updated for Ajavon et al. (2003).

The winds and temperatures used for transport and to calculate kinetic reaction rates in the CTM were specified from a 50-yr integration of the Finite-Volume General Circulation Model (FVGCM). The FVGCM uses a flux-form semi-Lagrangian transport code with a quasi-Lagrangian vertical coordinate (Lin 2004), which yields accurate computations of tracer transport (Lin and Rood 1996) and dynamical evolution (Lin and Rood 1997). A horizontal resolution of 2.5° × 2° (longitude by latitude) was used, with 55 model layers between the surface and 0.01 hPa. Physical tendencies are calculated using a version of the parameterization package of Kiehl et al. (1998). Drag resulting from the dissipation of a coarse spectrum of gravity waves with nonzero phase speeds is included, in order to improve the simulation of the upper stratosphere and mesosphere, using the method of Garcia and Boville (1994). The lower boundary sea surface temperatures and sea ice distributions were imposed from Rayner et al. (2003). The FVGCM can be extended to include trace gases; in this run, parameterized ozone and methane were added, using production and loss rates from the 2D simulations of Jackman et al. (1996). These did not interact with the model's radiation code.

Meteorological fields from a prior version of the FVGCM have been used in the GSFC CTM (Douglass et al. 2003), and also in simulations with the Global Modeling Initiative (GMI) CTM. Analysis and evaluation of the results attest to the credible representation of stratospheric climate and to the realism of transport, including the "age of air" (Strahan and Douglass 2004; Considine et al. 2004). Olsen et al. (2004) show that the exchange of mass and ozone between the stratosphere and troposphere is realistic compared with estimates derived from observations.

## 3. Observations of total column ozone and ozone profiles

Observations used here are made by the Total Ozone Mapping Spectrometer (TOMS) and Solar Backscatter Ultraviolet (SBUV) instruments. The first TOMS and SBUV were flown on the *Nimbus-7* satellite launched in 1978. The current TOMS instrument is on the *Earth Probe* satellite launched in 1996. Successor instruments to SBUV have been the SBUV-2 instruments on the National Oceanic and Atmospheric Administration (NOAA) satellites *NOAA-9*, *-11*, *-14*, and *-16* launched in 1985, 1989, 1996, and 2001, respectively. These data have been merged into a single consistent time series for total ozone (available online at http://code916.gsfc.nasa.gov/Data_services/merged). The data have been described and compared to other similar datasets by Fioletov et al. (2002). The data used here are processed using the version 8 TOMS and SBUV algorithms (Frith et al. 2004; Ahmad et al. 2004). The entire calibration histories of the TOMS and SBUV instruments have been reviewed in the process of producing the new version 8 data. These data are estimated to have a possible instrument drift uncertainty of slightly greater than 1% decade$^{-1}$ (unpublished estimate). The uncertainties quoted in the data analyses in this paper do not include this estimate. The SBUV profile datasets from the various instruments have been placed on a consistent calibration basis, allowing the construction of a merged profile dataset that is also available on the Web site above (see McPeters et al. 2004 and Bhartia et al. 2004 for more details).

## 4. The statistical time series model

The underlying physical model used in the statistical time series analysis is an extension of the basic physical model used by Stolarski et al. (1991). The physical model includes terms that represent the mean ozone and its seasonal cycle, the trend, the solar cycle, the QBO, and volcanic aerosol effects. The ozone is approximated by the following expression:

$$O_3(t) = \mu + \alpha \times \text{Chlorine} + \beta \times \text{QBO} + \gamma \times \text{Solar} + \delta_1 \times \text{El Chichon} + \delta_2 \times \text{Pinatubo} + \text{noise}. \quad (1)$$

The parameters $\mu$, $\alpha$, $\beta$, $\gamma$, $\delta_1$, and $\delta_2$ are to be estimated by regression analysis. Total ozone is represented by a mean $\mu$ and annual and semiannual harmonics. Likewise all other fitting parameters are represented by an annual mean plus annual and semiannual harmonics. Four seasonal harmonics are used for the upper-stratospheric profile. The characteristic shapes of the chlorine, solar, QBO, and volcanic terms are shown in Fig. 1. The QBO is modeled using the two-EOF decomposition (Wallace et al. 1993) and has been used in this type of analysis by Randel et al. (1995). The solar

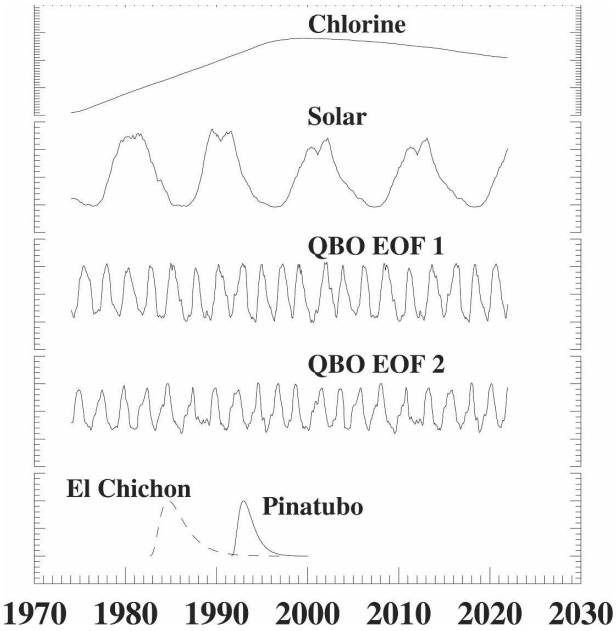


FIG. 1. Terms used in the statistical time series analysis.

term is proportional to the 10.7-cm radio flux measured at Ottawa, Canada.

We fit the volcanic aerosol terms for El Chichon and Pinatubo separately. The timing of the photochemical ozone response to the aerosol increase from a volcanic eruption depends upon the combination of transport of aerosols and photochemical processes that lead to ozone loss. We use the GSFC two-dimensional chemistry and transport model (2DCTM) to approximate the volcanic response functions. The 2DCTM has contributed to ozone assessments (e.g., Ajavon et al. 2003) has been compared with observations from many sources and has been used extensively for analysis of ozone trends (Jackman et al. 1996; Fleming et al. 1999). We use a time delay in the ozone response to the aerosol increase as calculated by 2DCTM to represent the aerosol in the statistical time series analysis. The El Chichon shape includes the response to the aerosols from Ruiz and other smaller volcanoes that erupted in the years after El Chichon, thus the recovery tail is long. We tested the shape of the aerosol term by fitting the difference between two 3DCTM simulations with and without aerosols. The overall shapes were similar.

The response term for chlorine accounts for the leveling off of the stratospheric chlorine confirmed by the time series of HCl obtained from the Halogen Occultation Instrument (HALOE) on the *Upper Atmosphere Research Satellite* (*UARS*; Anderson et al. 2000). Instead of a linear "trend" term in the time series analysis we use a quantity analogous to the equivalent effective stratospheric chlorine (EESC) described by Madronich and Velders (1998). We use the total inorganic chlorine mixing ratio plus 50 times the total inorganic bromine mixing ratio at 1 hPa in our simulations; we refer to this as effective chlorine (EC). At 1 hPa almost all of the chlorine and bromine have been converted to inorganic form. The CTM transport accounts for the age spectrum, which Schoeberl et al. (2003) have shown to be realistic. In contrast, the classical EESC is determined for the middle stratosphere where only about half of the chlorine and bromine are in inorganic form; this EESC is applied with a 3-yr lag to account for the mean age of air. The EC function is less sharply peaked than the EESC.

The EC in Fig. 1 increases linearly with time from the 1970s until ~1997; it is appropriate to use a linear trend as a surrogate for the effect of chlorofluorocarbons and halons on stratospheric ozone during this time period. The deviation from a linear trend in time as a result of cessation of the growth of atmospheric chlorine begins after 1995. We have now accumulated enough years beyond 1995 that it is appropriate to use the EC function in a time series analysis of observations. Any time series analysis will return trends that are biased toward smaller negative values if the time series analysis seeks a linear response to the chlorine perturbation and includes data beyond 1996. The functional form in Fig. 1 allows use of 7 more years of ozone data (or simulation results) to quantify the solar and aerosol effects and to lessen the possibility that random, interannual dynamic processes, not included in the physical model, will contribute to the calculated trends. The time series analysis tests whether the observations (or simulations) support a statistically significant response to the EC function. The coefficient determined for EC in the statistical analysis is the change in ozone per ppbv of EC. This coefficient can be expressed as DU ppbv$^{-1}$ EC [where 1 DU (Dobson unit) = $2.69 \times 10^{16}$ molecules of ozone per square centimeter] or % ppbv$^{-1}$ EC. It can be converted to a linear trend in ozone for the time period from the mid-1970s up to 1996 by multiplying by the linear trend in EC for that period (shown in Fig. 1) of 1.2 ppbv decade$^{-1}$. All uncertainties shown are $2\sigma$ estimates based on a bootstrap technique of rearranging the residuals from the time series fit.

## 5. Analysis of total column ozone

### *a. Global average*

A time series of the global average of the total column ozone would be the best dataset from which to diagnose ozone trends. Variability caused by transport of ozone is minimized by integration over the globe.

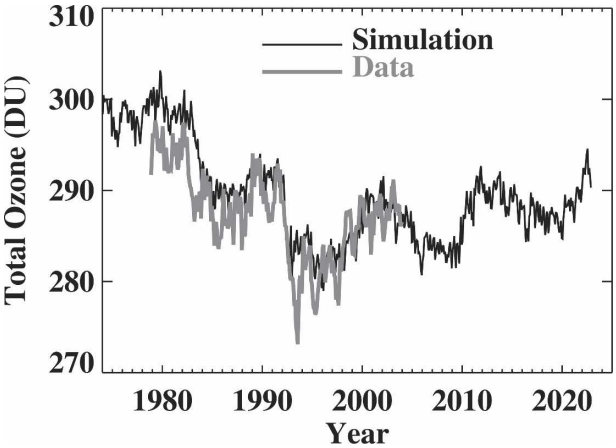


FIG. 2. Comparison of quasi-global (60°S–60°N) mean total ozone from simulation with merged ozone data from TOMS and SBUV. The black line is the deseasonalized model simulation. The gray line is the deseasonalized TOMS–SBUV merged total ozone data.

TABLE 1. Comparison of annually averaged responses to the chlorine–bromine term derived from time series analysis of simulated and observed total ozone. First column is the trend in DU ppbv$^{-1}$ change in EC. Second column is this number converted to equivalent trend, in DU decade$^{-1}$, from late 1978 to 1996. Third column is the trend converted to % decade$^{-1}$. Uncertainties are $2\sigma$ statistical deviations calculated from a bootstrap analysis of the residuals to the fit.

| | DU ppbv$^{-1}$ EC | DU decade$^{-1}$ | % decade$^{-1}$ |
|---|---|---|---|
| Observed 60°S–60°N | −3.1 ± 0.4 | −3.7 ± 0.5 | −1.3 ± 0.2 |
| Simulated 60°S–60°N | −5.8 ± 0.2 | −6.9 ± 0.2 | −2.4 ± 0.1 |
| Simulated 90°S–90°N | −7.9 ± 0.4 | −9.5 ± 0.5 | −3.2 ± 0.2 |

Since variability that is not accounted for by the time series analysis acts as noise and contributes to uncertainty in the results, quantification of the ozone trend, the solar cycle, or any process included in the time series analysis is more accurate when applied to a dataset that has been averaged over a sensible geophysical region. Ideally, we would integrate over the entire globe. This is easy to do in the simulation, but not possible with data because the TOMS and SBUV instruments use reflected sunlight for observations, hence making no measurements in the polar night. In addition, retrievals at very high solar zenith angles are strongly dependent on a priori information (Wellemeyer et al. 1997). Thus, TOMS and SBUV cannot measure a full seasonal cycle poleward of about 60° latitude. We compromise by forming a quasi-global mean that extends from 60°S to 60°N. We compare the simulated quasi-global mean to that calculated from observations in Fig. 2.

Figure 2 shows that there is a basic agreement for the quasi-global total between the simulation results and the data. There is a small offset (2.2 DU) between the 1979–2003 mean of the simulation and the observations. The observed peak-to-peak seasonal amplitude is 10.9 DU in the data compared with 8.6 DU in the simulation. We make more quantitative statements by applying the statistical approach described above to the output of the simulation and to the data.

Table 1 compares the sensitivity to EC ($\alpha$) and the trend for 1978–96 calculated from $\alpha$ for both the simulated ozone and the merged ozone data using simulation output and data from late 1978 to the end of 2003. The simulation appears to be nearly twice as sensitive to chlorine and bromine as the data for the 60°S–60°N average. We shall see below that the difference between the simulation and the data is best described as an offset of ~1% decade$^{-1}$ (or ~3 DU decade$^{-1}$), nearly independent of latitude. All conclusions concerning trends in this paper assume that the coefficient, $\alpha$, determined from the statistical analyses using all of the terms in Eq. (1) is really the sensitivity of the simulation of the atmosphere to the forcing due to chlorine and bromine. Table 1 also includes results for time series analysis of the global average total ozone (90°S–90°N) from the simulation. The global ozone change and trend in the simulation are substantially larger than that calculated for 60°S–60°N due to chlorine-catalyzed winter and spring ozone loss in the lower polar stratosphere. Table 2 includes the annual mean parameters obtained for solar, QBO, El Chichon, and Pinatubo in the time series analysis for the simulation and the observations, both averaged from 60°S to 60°N.

The simulation does not have a QBO while one does exist in the quasi-global mean data. A QBO term can be derived from the simulation, but it is not significant. A nonzero value for the QBO parameter arises when it is included because some of the unexplained variance projects onto the QBO term. Presence or absence of a QBO term in the time series analysis has no effect on the values of the other parameters derived from the simulation.

The sensitivity of the simulation to solar cycle agrees with that derived from the data within statistical uncertainty. Small, not significant, sensitivities are derived for the El Chichon aerosols (described in more detailed below). The simulation is less sensitive to the Pinatubo aerosols than observed (also described in more detail below). We tested the fit to the Pinatubo and El Chichon aerosols by comparing the CTM simulation to a similar simulation using the same dynamics and back-

TABLE 2. Comparison results for other terms in time series analysis for observed and simulated "global" total ozone (60°S–60°N). Solar term is in Dobson units per 100 units of the 10.7-cm radio flux at Ottawa (F10.7; these units are $10^{-2}$ W m$^{-2}$ Hz$^{-1}$). QBO term is in DU (100 m)$^{-1}$ s$^{-1}$. El Chichon and Pinatubo terms are in DU. All are annually averaged. Uncertainties are $2\sigma$ statistical deviations calculated from a bootstrap analysis of the residuals to the fit.

| | Solar [DU (100 units F10.7)$^{-1}$] | QBO [DU (100 m)$^{-1}$ s$^{-1}$] | El Chichon (DU) | Pinatubo (DU) |
|---|---|---|---|---|
| Observed | 5.2 ± 0.6 | 4.1 ± 1.1 | 0.7 ± 1.1 | −6.7 ± 1.1 |
| Simulated | 4.5 ± 0.3 | — | −1.2 ± 1.1 | −4.0 ± 1.1 |

ground aerosols. The shape obtained for the influence of each volcano was fit well with the function used from the 2DCTM results.

### b. Zonal mean ozone versus latitude

There is a small bias between the 60°S–60°N averages of the observed and simulated column ozone, but more information can be gained by examining the latitude dependence of the difference between the simulated total ozone and the merged total ozone dataset. Figure 3 shows a 25-yr time series of the difference as a function of latitude. The graph at the right shows the average bias between the simulation and the data. Although the quasi-global bias is near zero, we see that the simulation overestimates ozone poleward of 45° in the Northern Hemisphere and poleward of ~30° in the Southern Hemisphere. The simulation underestimates ozone at low to midlatitudes. Near the equator, the difference shows a quasi-biennial oscillation as the simulation does not have a QBO, but the mean difference is small and positive.

We apply the time series analysis used above to the zonal means of the simulated and observed total ozone as functions of latitude. Figure 4 shows the trends derived from late 1978 to 1996 from using the time series analysis including the EC function in Fig. 1 to fit the simulated and observed total ozone through the end of 2003 for the latitude range 60°S–60°N. The simulation shows a small, but significant negative trend in the equatorial region in disagreement with the data, which have no trend. The simulated trend in the Tropics results from a simple catalytic loss of ozone in the photochemical regime of the middle and upper stratosphere. It is not likely to be affected significantly by transport variability. The model does not account for the possibility of trends in tropospheric ozone. If the difference between the simulation and the data were because of upward trends in tropospheric ozone, the required amount would be ~10% decade$^{-1}$, or at least 5–6% decade$^{-1}$ to get the model within the uncertainty bounds of the trend derived from data for the 20°S–20°N tropical average. Part of the issue with the tropical trends calculated in the model is that the model-calculated ClO concentration in the Tropics is about 10%–15% higher than the measurements made by the Microwave Limb Sounder (MLS) instrument on *UARS* (Froidevaux et al. 2000). Outside the Tropics for southern latitudes the simulation also exhibits larger trends than are derived from data. The difference between the simulation and the data increases from ~1% to ~2% decade$^{-1}$ at 60°S latitude. For the latitude band from

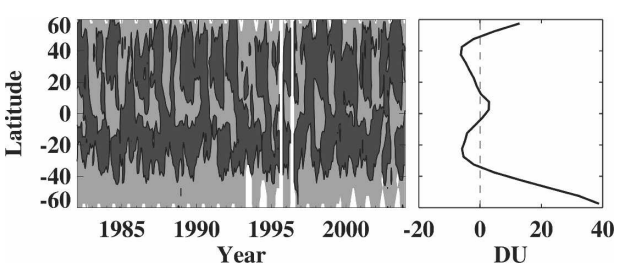


FIG. 3. Difference between the CTM simulation and TOMS–SBUV merged ozone dataset from 1979 to 2003. (left) Time-dependent latitude variation with light gray shaded areas indicating where the simulation is larger than the data and the dark gray shaded areas indicating where the simulation is less than the data. (right) Time average of the latitude-dependent difference.

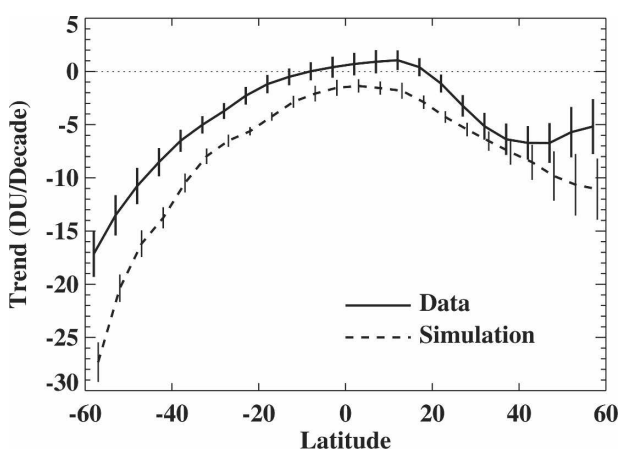


FIG. 4. Annual average trend in total ozone vs latitude calculated from the model and from the data. Trends are for the time period from late 1978 to 1996 calculated using data through 2003 and the EC function described in this paper. The $2\sigma$ uncertainties (vertical lines) account for the autocorrelation of the residual time series at each latitude.

55° to 60°S the simulation result is −30 ± 4 DU decade$^{-1}$ compared to −17 ± 3 DU decade$^{-1}$ for the data. The difference between these two values is clearly greater than their combined $2\sigma$ uncertainties. In the northern midlatitudes the trends derived from the simulation agree with those derived from the data to within statistical uncertainty although the simulation always has a more negative trend than the data.

The FVGCM winds have interannual variability that introduce uncertainty into the results for trends derived from CTM fields. The uncertainty in the trends from the simulation is greater than that derived from the observations poleward of 40°N. This is because the simulation exhibits larger dynamical interannual variability than does the atmosphere in this region (discussed below). The uncertainty makes it difficult to attribute trends to the chemical changes as a result of the changing chlorine–bromine compounds. This is exactly the same problem faced with real atmospheric data. We have more complete knowledge about the simulation than we do about the atmosphere because we also have the online parameterized ozonelike tracer that can be used to fully account for the effects of interannual variability in the dynamics. This allows us to evaluate the problem and draw some conclusions about limitations of trend derivation in the atmosphere (see the next section).

Figure 5 shows the annual average solar cycle coefficient derived from the model and the data for the time period 1978–2003. The $2\sigma$ uncertainties are derived from a bootstrap technique. The residuals are scrambled in 3-month blocks and then refit to determine the solar cycle that may be accidentally mimicked by the interannual variability of the dynamics. Although the sensitivity of the simulated total ozone to the solar cycle is slightly larger than that derived from observations, this analysis shows that the simulation and observations exhibit the same sort of solar response within the large uncertainties. Note that the GCM simulation did not include variable UV forcing over a solar cycle. The results for the comparison of the CTM simulation to data for solar cycle are quite good. The statistical analysis used data through the end of 2003 for both the simulation and the measurements. A similar analysis using data only through 1996 (the period of linear trends) yielded less agreement for northern midlatitudes. Extension of the analysis of the simulation beyond 2003 yielded essentially the same result for the northern midlatitude solar cycle as shown in Fig. 5.

Figure 6 shows sensitivity to Pinatubo aerosols derived from the time series analysis of observed and simulated total ozone. The fit to the observations indicates a significant effect poleward of 40°N reaching

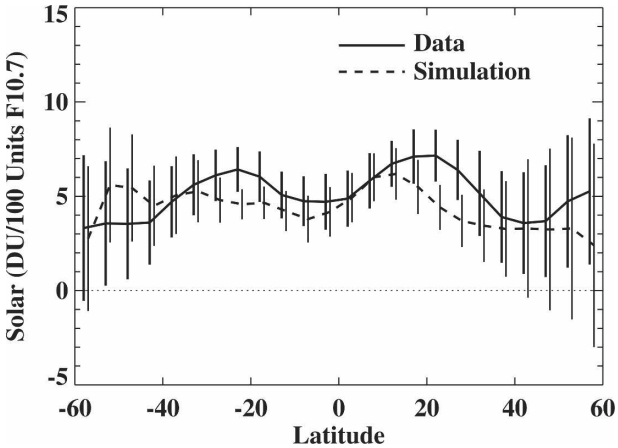


FIG. 5. Annual mean solar cycle coefficient derived from the time series analysis of simulated and observed total ozone as a function of latitude. Uncertainties are $2\sigma$ and are derived from a bootstrap analysis.

20 DU for the 55°–60°N latitude band. There is virtually no effect in the Southern Hemisphere. The fit to the simulation shows the reverse with a maximum effect in the Southern Hemisphere poleward of 40°S. The simulation shows virtually no effect in the Northern Hemisphere. To examine this further we reran the CTM for the Pinatubo time period using background aerosols. We take the difference between these two simulations and then apply the time series analysis to quantify directly the simulation response to Pinatubo. The result is shown as the dashed line in the right panel in Fig. 6. It demonstrates an effect in both hemispheres as would be expected from the input aerosol distributions and the chemistry of the atmosphere as specified in the CTM. This suggests that the lack of a northern midlatitude Pinatubo effect in the analysis of the full CTM run is due to a failure of the analysis rather than the absence of an effect. To test this we can use the online ozonelike tracer to account for interannual variability by subtracting its variability from a mean seasonal cycle from the full model simulation. The result of the time series analysis with interannual variability removed is shown as the dashed line in the right panel in Fig. 6. We see that the Pinatubo effect can be retrieved from a CTM simulation with both solar cycle and volcanic aerosols if the physical model in the statistical analysis accounts for interannual variability. The time series analysis of the simulated ozone at high northern latitudes mixes interannual variability with the Pinatubo aerosols. Removal of the interannual variability reveals the simulation's true response to the aerosols. The Pinatubo effect calculated from data in the northern midlatitudes is subject to similar uncertainty limits due to interannual variability. The error bars shown in

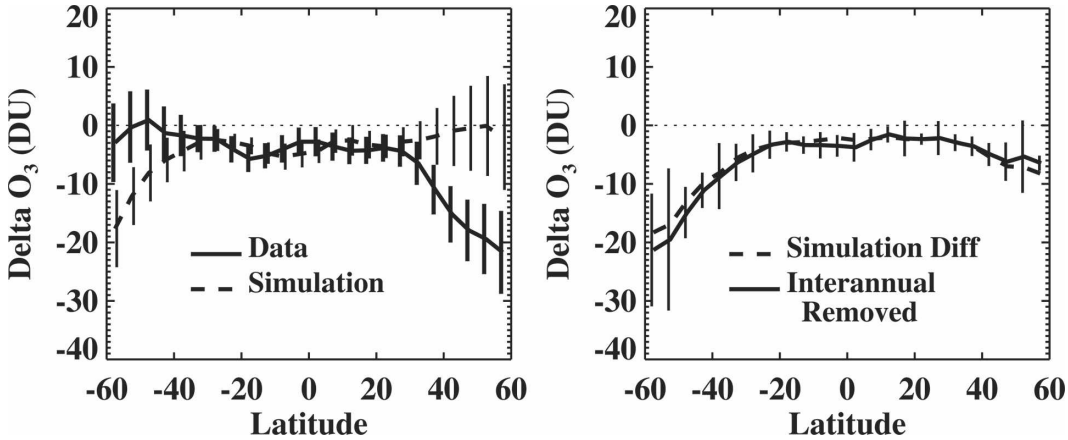


FIG. 6. (left) Maximum annually averaged Pinatubo effect derived from time series analysis of simulated and observed total ozone (dashed and solid black lines with $2\sigma$ uncertainties). (right) Dashed line is the Pinatubo effect derived from the difference between simulations with and without Pinatubo aerosols. Solid line with $2\sigma$ uncertainties is the Pinatubo effect derived from the simulation accounting for interannual dynamical variability using the online ozonelike tracer.

Fig. 6 attempt to represent these uncertainty limits, but may be imperfect because it only takes one or two unusually cold or warm winters to seriously compromise the correct determination of the volcanic effect.

The result from the model analysis of the Pinatubo effect in the Northern Hemisphere suggests that the problem with the lack of a Pinatubo effect in the Southern Hemisphere data may be a failure of the analysis. The combination of solar cycle and volcanic aerosols in a time-varying meteorology may mask the effect. The addition of more years to a dataset will help to better define the solar cycle, but will not address the time-varying meteorology and how it might have confused the analysis for the short-lived volcanic perturbation. The only way we can do that is to have a better dynamical surrogate to remove interannual variability from the data.

### c. *Variability and trend detection*

We have seen that dynamical variability can interfere with detection of volcanic effects. In this section we further examine the effects of interannual variability on the detection of trends. We use the online ozonelike tracer to separate dynamical and chemical components of the trend in our simulation. To do this, we remove the seasonal cycle from the parameterized ozone and then subtract the deviations of the residual from the simulated ozone. Since both were calculated using the same transport, the variability due to that transport is effectively removed. We do not have a surrogate for the real atmosphere that is as accurate. We use this analysis of the simulation to attempt to derive limits on the dynamical contributions to trend in the real atmosphere.

The variability of ozone in our CTM simulation includes contributions from chlorine–bromine change, solar cycle UV variation, volcanic aerosols, and interannual variability of dynamics. To understand the limits that interannual variability of dynamics puts on ozone trend detection, we compare the variability of the simulation to that of the data. To do this, we first fit the simulation and the data with a time series model for the mean, seasonal cycle, chlorine–bromine, solar UV, and aerosols. The residual variability from this fit is then the "noise" term. We do this for the zonal mean at each latitude for each month. The ratio of the standard deviation of this residual for the simulation to that for the data is shown in Fig. 7 versus month and latitude.

The ratio is close to unity over much of the globe, but is significantly higher in the late spring northern high latitudes. Over much of the globe, the simulation has a good representation of the statistics of interannual variability. From this we can derive some uncertainties concerning the dynamical component of ozone change. We have to be cautious because the simulation will somewhat overestimate the uncertainty due to the dynamical trend at high northern latitudes during the winter and early spring.

Figure 8 shows a calculation of the uncertainty in the trend derived from the CTM simulation for the trend from 1979 to the end of 1996. The left panel shows the uncertainty in trend ($2\sigma$) using data only through the end of 1996. The right panel shows the uncertainty using data through the end of 2003. These uncertainties were calculated assuming that the residual time series is fit reasonably well by autocorrelated noise with lag of 1 month. We can use the standard deviation of this re-

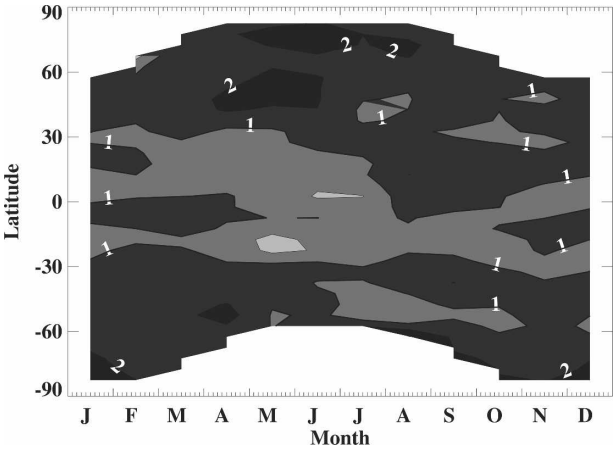


FIG. 7. Ratio of standard deviation of the simulation to that from observations as a function of latitude and season. Black regions are where simulation has more than twice the standard deviation as the data. Light gray regions are where the simulation has less than half the standard deviation of the data.

sidual series with the autocorrelation coefficient to calculate the standard deviation of the linear trends that would occur for a time series of a given length:

$$\sigma_{\text{trend}} = \sigma_{\text{resid}}/(1 - \phi)/n^{3/2},$$

where $\sigma_{\text{resid}}$ is the standard deviation of the residual time series after the removal of specific terms with surrogates, $\phi$ is the autocorrelation coefficient for a 1-month lag, $n$ is the number of months in the time series record, and $\sigma_{\text{trend}}$ is the resulting standard deviation of the uncertainty in the trend (Weatherhead et al. 1998). These calculations are shown as the gray-shaded areas in Fig. 8 as $2\sigma$ uncertainties. The extension of the dataset leads to smaller potential dynamical trends of what might be called the "accidental" type, that is, dynamical trends that occur because of variability over a short time record. These are to be differentiated from dynamical trends that might be forced by underlying climate changes such as those due to increasing greenhouse gases or due to feedback from the ozone changes themselves.

Also shown in Fig. 8 is the realization of the chemical and dynamical trend for this simulation with its specific interannual variability from the GCM dynamics. The dynamical trend was obtained by using the statistical time series analysis to fit the online ozonelike tracer. The chemical trend was obtained by fitting the full CTM simulation with the online ozonelike tracer deviations subtracted to remove dynamical variability. In this particular case the dynamical trend determined using the simulation output only through 1996 was negative and added to the chemical trend to get the overall trend. When output through 2003 was used, the dynamical trend was small and had little impact on the determination of the chemical component. This indicates, at least for this model simulation, that the inclusion of data through 2003 and the use of the chlorine–bromine-forcing function resulted in the correct retrieval of the chlorine–bromine sensitivity by the time series analysis.

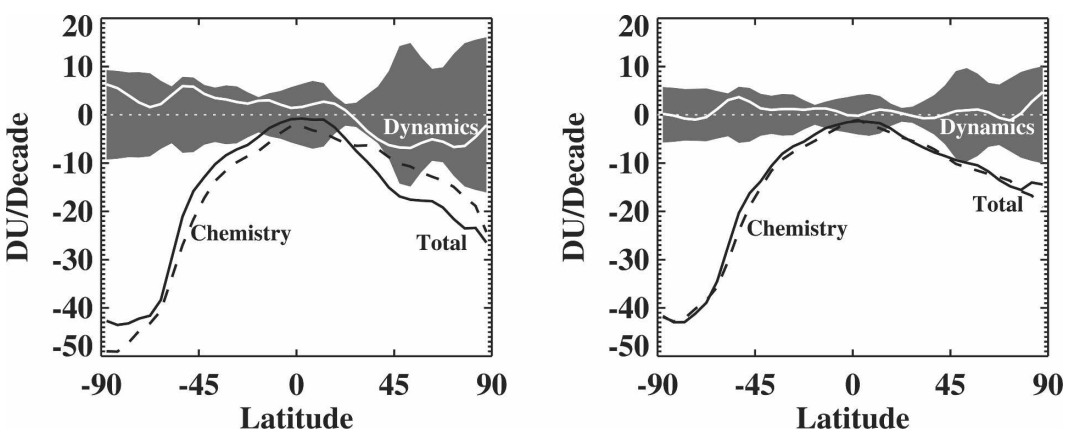


FIG. 8. Annual average trends calculated in CTM and GCM for total ozone as a function of latitude for the time period from 1979 to 1997. The gray shaded area represents the $2\sigma$ uncertainties in the dynamical component calculated from the standard deviation and autocorrelation of the online tracer time series after removal of seasonal cycle. The white line through the shaded area is the dynamical contribution to the trend calculated from the online ozonelike tracer. The dashed line is the chemical contribution to the trend calculated from the difference between the CTM full-chemistry ozone and the online ozonelike tracer. The solid black line is the sum of the chemical and dynamical components. (left) The trend fitted through 1997. (right) The trend through 1997 using data through 2003 and the EC function in Fig. 1.

## 6. Analysis of profile ozone

We can gain more insight into performance of the simulation by comparing observed and simulated ozone profiles. We will focus on the trends at northern midlatitudes and compare to the results derived in the Harris et al. (1998) study.

In 1997 the Stratospheric Processes and their Role in Climate (SPARC) project called together an Ozone Trends Panel to study our knowledge of trends in the altitude profile of ozone. In the trends chapter of this report (Harris et al. 1998), a summary was constructed of the trends from four different instrument systems: the Stratospheric Aerosol and Gas Experiment (SAGE), Umkehr, SBUV, and ozonesondes. This was only possible at northern midlatitudes where there were sufficient Umkehr and ozonesonde measurements. The summary they constructed is shown in Fig. 9 as the white line and the shaded areas. They found two maxima in negative trend, one in the upper stratosphere at about 40-km altitude and the other in the lower stratosphere centered at about 15-km altitude. These trends used data from 1980 to the end of 1996. We have sampled our CTM simulation for the same time period and obtained a similar result with maximum negative trend in both the upper and lower stratosphere. The CTM trends are both larger than those found by the SPARC panel. They are shown by the solid black line in Fig. 9 with $2\sigma$ uncertainty bounds of the statistical time series analysis of the CTM output.

It is expected that the trend in the upper stratosphere is larger in the simulation than in the observations. Two factors contribute. Comparisons of methane observations from HALOE show that methane simulated using winds from FVGCM is generally low compared with observations. Douglass et al. (2004) found that the simulated ClO is generally high compared with observations from the MLS (Livesey et al. 2003) as a result of reduced formation of the chlorine reservoir HCl. This deficiencies in the upper stratosphere make the simulation more sensitive to an increase in upper-stratospheric chlorine. The second factor contributing to the CTM sensitivity to upper-stratospheric chlorine change is the lack of a realistic temperature trend. The CTM simulation used temperatures and winds from a 50-yr run of the FVGCM with constant amounts of $CO_2$ and ozone in the radiation code. The result is a stationary time series of upper-stratospheric temperatures that is not consistent with analyses of temperature data (e.g., Ramaswamy et al. 1999). The observed decrease in stratospheric temperature in the upper stratosphere should lead photochemically to an increase in ozone

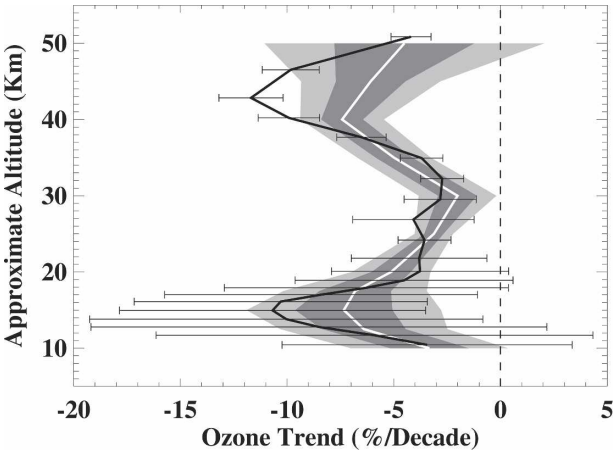


FIG. 9. Comparison of CTM-derived trends to those from 1997 SPARC Ozone Trends Panel for the time period 1980–96. The thick white line is the mean trend from four data sources reported in Harris et al. (1998). Dark and light gray shading indicates the $1\sigma$ and $2\sigma$ uncertainties. The heavy black line is the trend deduced from the CTM simulation for the same time period. The light black error bars are the $2\sigma$ uncertainties of the model trend.

and a reduction in the negative trend due to the chlorine increase. If the CTM simulation had a negative temperature trend in the upper stratosphere, the result would have been a smaller ozone trend.

The lower stratosphere presents a more interesting problem for the deduction of ozone trends. Figure 10 shows the time series from the CTM simulation for ozone mixing ratio at 118 hPa or about 15-km altitude. The series is dominated by a seasonal cycle. Removal of the average seasonal cycle leaves the deseasonalized residual in the bottom panel in Fig. 10. The trend in this

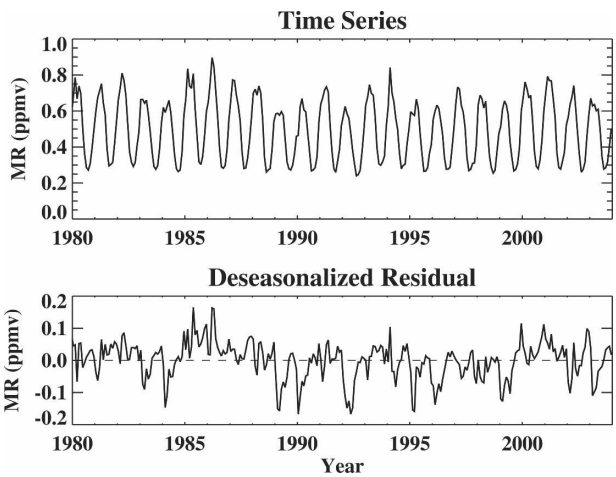


FIG. 10. (top) Time series from CTM simulation for the period 1980–2004 at 118 hPa (~15 km). (bottom) The residual after subtraction of the seasonal cycle.

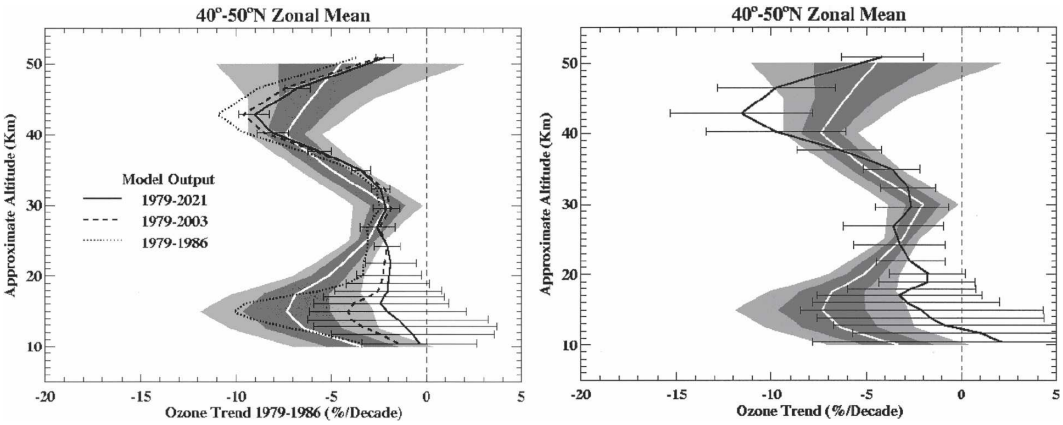


FIG. 11. (left) Zonal mean trends calculated for the latitude band between 40° and 50°N from data and the CTM. The white line is the mean from the data reported in Harris et al. (1998) and the gray shaded areas indicate $1\sigma$ and $2\sigma$ uncertainties. The black lines indicate deductions of trend from the CTM simulation using output from 1980 to 1996, 2003, and 2021, respectively. (right) SPARC data analysis overlaid with the solid black line calculated from the trend analysis of the CTM simulation with interannual variability removed using the online ozonelike tracer.

residual time series is not evident to the eye, but the time series analysis produces a statistically significant trend for the time period from 1980 to 1996 (as shown in Fig. 9).

When longer time periods are considered, the picture changes somewhat. Figure 11 (left panel) repeats the SPARC results and superposes three results from the CTM simulation. These are all from the same simulation but include simulated ozone from 1980 to 1996, 2003, and 2021. The statistical time series analysis uses the EC function from Fig. 1, along with seasonal, solar cycle, and volcanic aerosol terms to establish a best fit to the simulated ozone. The figure reports the trend obtained for the period 1980–96 using each length of the simulated time series. The dotted line repeats the linear trend obtained for data from 1980 to 1996. The dashed line shows the calculation with data considered through the end of 2003 to obtain the best fit for the trend. The solid line with $2\sigma$ uncertainty bars shows the resulting trend when the data from the entire CTM simulation is used to establish the best fit to the chlorine–bromine function.

As we include output from the CTM for a longer simulation period, the trend deduced in the lower stratosphere becomes smaller and less significant. The best estimate of trend in the lower stratosphere of the northern midlatitudes using the entire model output is of the order of 2%–3% decade$^{-1}$ spread over a broad altitude layer. This highlights the difficulty in deducing trends in the lower stratosphere from actual data when the time series are short. The longer the time series, the better it will be for trend determination. Finally, Fig. 11 (right panel) shows the ozone trend from the statistical model applied to the simulation for 1979–2003 using the online ozonelike tracer to account for dynamical variability. This result is nearly identical to that obtained using the statistical model for 1979–2021. This confirms that including a realistic surrogate for dynamical variability in the statistical model will improve determination of the chemical trend from a limited dataset.

## 7. Summary and conclusions

We have carried out a simulation of the full chemistry of stratospheric ozone in our CTM for the last 30 yr and for 20 yr into the future. This simulation used imposed mixing ratio boundary conditions for the evolution of chlorine–bromine-containing compounds as well as for methane and nitrous oxide. The simulation also included solar cycle variations of the solar flux of ultraviolet radiation and time-dependent volcanic aerosol variations. A goal of this simulation was to evaluate our knowledge concerning the chemical and dynamical sensitivity of the stratosphere to past and future perturbations.

We used the winds from the FVGCM because they had good overall dynamical characteristics for long-term stratospheric ozone simulations (e.g., "age of air" and stratosphere–troposphere exchange). The resulting simulation had the following properties when compared to TOMS and SBUV ozone data.

### *a. Global total column ozone (60°S–60°N)*

The bias between the simulation and the quasi-global total column ozone was about 1% or 2.8 DU with the

simulation slightly larger than the data. The simulation had a smaller seasonal amplitude (9.4 DU) than did the data (14.4 DU). A statistical time series analysis was applied to both the data and to the simulation sampled exactly as the data. This time series analysis, applied to the time period from late 1978 to the end of 2003 indicated that the quasi-global ozone in the simulation was more sensitive to the chlorine–bromine term than was the data. The chlorine–bromine sensitivity was determined using a functional form analogous to equivalent effective stratospheric chlorine. This functional form represents a near-linear increase from the mid-1970s to about 1996 and then a slow down and leveling off as manufacture and release of ozone-depleting substances has come under the control of the provisions of the Montreal Protocol. The shape is somewhat like the "hockey stick" used in some other analyses. The solar term derived by this analysis for the simulation was in agreement with that derived from the data. The simulation appeared to be somewhat less sensitive than the data to Pinatubo aerosols on the global scale.

### *b. Latitude-dependent total column ozone*

The zonal mean total ozone in the simulation showed a latitude-dependent bias with respect to the data. The latitude dependence of the chlorine–bromine term derived from the simulation agreed with that derived from the data, except in the southern mid- to high latitudes where the simulation was more sensitive. The solar term was consistent with the data as a function of latitude. The term derived from this analysis for Pinatubo in the CTM simulation provided an interesting result. The Pinatubo aerosol effect did not show up at northern midlatitudes. This was surprising because the subtraction of the simulation with and without aerosol enhancement due to Pinatubo indicates that the simulation did respond to the aerosols as expected. Using the online ozonelike tracer as a dynamical surrogate removed this problem and the Pinatubo effect showed up as expected. We speculate that this type of effect may be responsible for the apparent lack of a Pinatubo effect in the total ozone data for the Southern Hemisphere.

### *c. Altitude profile of ozone concentration*

The simulation was compared to the trends in ozone profile derived in the SPARC panel Harris et al. (1998) report at northern midlatitudes. The simulation resulted in a larger sharp peak in the negative trend in the lower stratosphere than reported by SPARC for the time period from 1980 to 1996. We extended the analysis of the CTM simulation for the trend from 1980 to 1996 by using the model output beyond that time period to achieve a better fit to the expected ozone time signature. When we did this the sharp peak was significantly reduced. These results indicate that the expected lower-stratospheric response in the northern midlatitudes is spread more generally throughout the lower-stratospheric region.

The results reported in this paper highlight some important issues concerning statistical trend analyses of stratospheric ozone. The interannual variability of the GCM dynamics makes it more difficult to determine how the CTM responded to various perturbations. This is similar to what happens in the real atmosphere. We have illustrated several difficulties in determining trends, solar cycle, and volcanic effects from data extending from the beginning of the satellite era in late 1978 to 1996 or 1997. These difficulties can be removed by extending the dataset to 2003 or a little later or by the use of a good dynamical surrogate. These results indicate that the trend derived for the period up to 1997 can be obtained from a longer dataset without significant contributions from an apparent dynamical component due to the interannual variation of the meteorology of the stratosphere. We have not addressed the possibility that a forced component due to greenhouse gas trends and warming of the troposphere contributes to the trend. Such a trend should eventually be separable from a chlorine–bromine component as the chlorine and bromine are removed from the atmosphere while the greenhouse gases continue to increase. A second type of forced dynamical trend is one due to the change in ozone itself. This feedback could enhance or diminish the apparent trend and is a part of the response of ozone to chlorine–bromine changes.

*Acknowledgments.* We thank the Goddard Modeling and Assimilation Office for the development of the general circulation model and for producing the 50-yr simulation used in this work. We further thank David Considine for the development of the aerosol climatology. This work was funded by NASA's Atmospheric Chemistry Modeling and Analysis Program.

## REFERENCES

Ahmad, S., J. Johnson, R. D. McPeters, and P. K. Bhartia, 2004: TOMS version-8 data products and their applications. *Proc. Quadrennial Ozone Symp.,* Kos, Greece, International Ozone Commission, 287–288.

Ajavon, A.-L. N., D. L. Albritton, G. Megie, and R. T. Watson, Eds., 2003: Scientific assessment of ozone depletion: 2002. WMO Global Ozone Research and Monitoring Project Rep. 47, Geneva, Switzerland.

Anderson, D. E., Jr., and S. A. Lloyd, 1990: Polar twilight UV-visible radiation field: Perturbations due to multiple scatter-

ing, ozone depletion, stratospheric clouds, and surface albedo. *J. Geophys. Res.,* **95,** 7429–7434.

Anderson, J., J. M. Russell, S. Solomon, and L. E. Deaver, 2000: Halogen occultation experiment confirmation of stratospheric chlorine decreases in accordance with the Montreal Protocol. *J. Geophys. Res.,* **105,** 4483–4490.

Bhartia, P. K., C. G. Wellemeyer, S. L. Taylor, N. Nath, and A. Gopolan, 2004: Solar backscatter ultraviolet (SBUV) version 8 profile algorithm. *Proc. Quadrennial Ozone Symp.,* Kos, Greece, International Ozone Commission, 295–296.

Brueckner, G. E., K. L. Edlow, L. E. Floyd IV, J. L. Lean, and M. E. VanHoosier, 1993: The Solar Ultraviolet Spectral Irradiance Monitor (SUSIM) Experiment on board the Upper Atmosphere Research Satellite (UARS). *J. Geophys. Res.,* **98,** 10 695–10 712.

Chandra, S., J. L. Lean, O. R. White, D. K. Prinz, G. J. Rottman, and G. E. Brueckner, 1995: Solar UV irradiance variability during the declining phase of the solar cycle 22. *Geophys. Res. Lett.,* **22,** 2481–2484.

Considine, D. B., A. R. Douglass, P. S. Connell, D. E. Kinnison, and D. A. Rotman, 2000: A polar stratospheric cloud parameterization for the global modeling initiative three-dimensional model and its response to stratospheric aircraft. *J. Geophys. Res.,* **105,** 3955–3973.

——, P. S. Connell, D. J. Bergmann, D. A. Rotman, and S. E. Strahan, 2004: Sensitivity of global modeling initiative model predictions of Antarctic ozone recovery to input meteorological fields. *J. Geophys. Res.,* **109,** D15301, doi:10.1029/2003JD004487.

Douglass, A. R., and S. R. Kawa, 1999: Contrast between 1992 and 1997 high-latitude spring Halogen Occultation Experiment observations of lower stratospheric HCl. *J. Geophys. Res.,* **104,** 18 739–18 754.

——, M. R. Schoeberl, S. R. Kawa, and E. V. Browell, 2001: A composite view of ozone evolution in the 1995–1996 northern winter polar vortex developed from airborne lidar and satellite observations. *J. Geophys. Res.,* **106,** 9879–9895.

——, ——, R. B. Rood, and S. Pawson, 2003: Evaluation of transport in the lower tropical stratosphere in a global chemistry and transport model. *J. Geophys. Res.,* **108,** 4259, doi:10.1029/2002JD002696.

——, R. S. Stolarski, S. E. Strahan, and P. J. Connell, 2004: Radicals and reservoirs in the GMI chemistry and transport model: Comparison to measurements. *J. Geophys. Res.,* **109,** D16302, doi:10.1029/2004JD004532.

Fioletov, V., G. Bodeker, A. Miller, R. McPeters, and R. Stolarski, 2002: Global and zonal total ozone variations estimated from ground-based and satellite measurements: 1964-2000. *J. Geophys. Res.,* **107,** 4647, doi:10.1029/2001JD001350.

Fiore, A., D. J. Jacob, H. Liu, R. M. Yantosca, T. D. Fairlie, and Q. Li, 2003: Variability in surface ozone background over the United States: Implications for air quality policy. *J. Geophys. Res.,* **108,** 4787, doi:10.1029/2003JD003855.

Fleming, E. L., C. H. Jackman, R. S. Stolarski, and D. B. Considine, 1999: Simulation of stratospheric tracers using an improved empirically based two-dimensional model transport formulation. *J. Geophys. Res.,* **104,** 23 911–23 934.

Frith, S., R. Stolarski, and P. K. Bhartia, 2004: Implication of version 8 TOMS and SBUV data for long-term trend analysis. *Proc. Quadrennial Ozone Symp.,* Kos, Greece, International Ozone Commission, 65–66.

Froidevaux, L., J. W. Waters, W. G. Read, P. S. Connell, D. E. Kinnison, and J. M. Russell III, 2000: Variations in the free chlorine content of the stratosphere (1991–1997): Anthropogenic, volcanic, and methane influences. *J. Geophys. Res.,* **105,** 4471–4481.

Fusco, A. C., and M. L. Salby, 1999: Interannual variations of total ozone and their relationship to variations of planetary wave activity. *J. Climate,* **12,** 1619–1629.

Garcia, R. R., and B. A. Boville, 1994: Downward control of the mean meridional circulation and temperature distribution of the polar winter stratosphere. *J. Atmos. Sci.,* **51,** 2238–2245.

Hadjinicolaou, P., A. Jrrar, J. A. Pyle, and L. Bishop, 2002: The dynamically driven long-term trend in stratospheric ozone over northern middle latitudes. *Quart. J. Roy. Meteor. Soc.,* **128,** 1393–1412.

Harris, N., R. Hudson, and C. Phillips, Eds., 1998: Assessment of trends in the vertical distribution of ozone. SPARC Rep. 1, WMO-Ozone Research and Monitoring Project Rep. 43, 120 pp.

Hood, L. L., J. P. McCormack, and K. Labitzke, 1997: An investigation of dynamical contributions to midlatitude ozone trends in winter. *J. Geophys. Res.,* **102,** 13 079–13 093.

Jackman, C. H., E. R. Fleming, S. Chandra, D. B. Considine, and J. E. Rosenfield, 1996: Past, present and future modeled ozone trends with comparison to observed trends. *J. Geophys. Res.,* **101,** 28 753–28 767.

Kiehl, J. T., J. J. Hack, G. B. Bonan, B. A. Boville, D. L. Williamson, and P. J. Rasch, 1998: The National Center for Atmospheric Research Community Climate Model: CCM3. *J. Climate,* **11,** 1131–1149.

Lin, S.-J., 2004: A vertically Lagrangian finite-volume dynamical core for global models. *Mon. Wea. Rev.,* **132,** 2293–2307.

——, and R. B. Rood, 1996: Multidimensional flux form semi-Lagrangian transport schemes. *Mon. Wea. Rev.,* **124,** 2046–2070.

——, and ——, 1997: An explicit flux-form semi-Lagrangian shallow water model on the sphere. *Quart. J. Roy. Meteor. Soc.,* **123,** 2477–2498.

Livesey, N. J., and Coauthors, 2003: The UARS microwave limb sounder version 5 data set: Theory, characterization, and validation. *J. Geophys. Res.,* **108,** 4378, doi:10.1029/2002JD002273.

Logan, J. A., 1999: An analysis of ozonesonde data for the troposphere: Recommendations for testing 3-D models and development of a gridded climatology for tropospheric ozone. *J. Geophys. Res.,* **104,** 16 115–16 149.

Madronich, S., and G. J. M. Velders, 1998: Halocarbon scenarios for the future ozone layer and related consequences. Scientific assessment of ozone depletion: 1998, WMO Rep. 44, World Meteorological Organization Global Ozone Research and Monitoring Project, 11.1–11.36.

McPeters, R., C. Wellemeyer, and A. Ahn, 2004: The validation of version 8 ozone profiles: Is SBUV ready for prime time? *Proc. Quadrennial Ozone Symp.,* Kos, Greece, International Ozone Commission, 113–114.

Olsen, M. A., M. R. Schoeberl and A. R. Douglass, 2004: Stratosphere–troposphere exchange of mass and ozone. *J. Geophys. Res.,* **109,** D24114, doi:10.1029/2004JD005186.

Petzoldt, K., 1999: The role of dynamics in total ozone deviations from their long-term mean over the Northern Hemisphere. *Ann. Geophys.,* **17,** 231–241.

Ramaswamy, V., and Coauthors, 1999: Stratospheric temperature trends: Observations and model simulations. *Rev. Geophys.,* **39,** 71–122.

Randel, W. J., F. Wu, J. M. Russell III, J. W. Waters, and L. Froidevaux, 1995: Ozone and temperature changes in the strato-

sphere following the eruption of Mount Pinatubo. *J. Geophys. Res.,* **100,** 16 753–16 764.

——, ——, and R. S. Stolarski, 2002: Changes in column ozone correlated with the stratospheric EP flux. *J. Meteor. Soc. Japan,* **80,** 849–862.

Rayner, N. A., D. E. Parker, E. B. Horton, C. K. Folland, L.V. Alexander, D. P. Rowell, E. Kent, and A. Kaplan, 2003: Global analyses of sea surface temperature, sea ice, and night marine air temperature since the late nineteenth century. *J. Geophys. Res.,* **108,** 4407, doi:10.1029/2002JD002670.

Salby, M. L., and P. F. Callaghan, 2002: Interannual changes of the stratospheric circulation: Relationship to ozone and tropospheric structure. *J. Climate,* **15,** 3673–3685.

Sander, S. P., and Coeditors, 2003: Chemical kinetics and photochemical data for use in atmospheric studies. Jet Propulsion Laboratory Publication 02-25, Jet Propulsion Laboratory, Pasadena, CA, 334 pp.

Schoeberl, M. R., A. R. Douglass, Z. K. Zhu, and S. Pawson, 2003: A comparison of the lower stratospheric age spectra derived from a general circulation model and two data assimilation systems. *J. Geophys. Res.,* **108,** 4113, doi:10.1029/2002JD002652.

Stolarski, R. S., P. Bloomfield, R. D. McPeters, and J. R. Herman, 1991: Total ozone trends deduced from *Nimbus-7* TOMS data. *Geophys. Res. Lett.,* **18,** 1015–1018.

——, and Coauthors, 1995: 1995 scientific assessment of the atmospheric effects of stratospheric aircraft. NASA Ref. Publ. 1381, NASA, 105 pp.

Strahan, S. E., and A. R. Douglass, 2004: Evaluating the credibility of transport processes in simulations of ozone recovery using the Global Modeling Initiative three-dimensional model. *J. Geophys. Res.,* **109,** D05110, doi:10.1029/2003JD004238.

Wallace, J. M., R. L. Panetta, and J. Estberg, 1993: Representation of the equatorial stratospheric quasi-biennial oscillation in EOR phase space. *J. Atmos. Sci.,* **50,** 1751–1762.

Weatherhead, E. C., and Coauthors, 1998: Factors affecting the detection of trends: Statistical considerations and application to environmental data. *J. Geophys. Res.,* **103,** 17 149–17 161.

Weiss, A. K., J. Staehelin, C. Appenzeller, and N. R. P. Harris, 2001: Chemical and dynamical contributions to ozone profile trends of the Payerne (Switzerland) balloon soundings. *J. Geophys. Res.,* **106,** 22 685–22 694.

Wellemeyer, C. G., S. L. Taylor, C. J. Seftor, R. D. McPeters, and P. K. Bhartia, 1997: A correction for total ozone mapping spectrometer profile shape errors at high latitude. *J. Geophys. Res.,* **102,** 9029–9038.

Ziemke, J. R., S. Chandra, R. D. McPeters, and P. A. Newman, 1997: Dynamical proxies of column ozone with applications to global trend models. *J. Geophys. Res.,* **102,** 6117–6129.